AECL-5991

ATOMIC ENERGY OF CANADA LIMITED

L'ÉNERGIE ATOMIQUE DU CANADA LIMITÉE

ELASTIC PLASTIC FRACTURE MECHANICS

by

L.A. SIMPSON

Whiteshell Nuclear Research Establishment

Pinawa, Manitoba

July 1978

ATOMIC ENERGY OF CANADA LIMITED

ELASTIC PLASTIC FRACTURE MECHANICS

by

L.A. Simpson

Whiteshell Nuclear Research Establishment
Pinawa, Manitoba, ROE 1LO
July 1978

AECL-5991

Mécanique des fractures élastiques linéaires

par

L.A. Simpson

Résumé

L'application de la mécanique des fractures élastiques linéaires à la stabilité des fissures dans les structures fragiles est maintenant bien connue et très employée. Cependant, dans de nombreux matériaux structurels, la propagation des fissures s'accompagne d'une plasticité considérable à l'extrémité des fissures qui invalide l'emploi de la mécanique susmentionnée. C'est pourquoi, les recherches actuelles dans le domaine de la mécanique des fractures ont pour but de développer des paramètres permettant de prédire la propagation des fissures dans des conditions d'élasticité et de plasticité. Les concepts étudiés comprennent des méthodes fondées sur l'ouverture et le déplacement critique des fissures et des techniques recourant à l'intégrale J et à la courbe R. Ce rapport sert d'introduction à ces concepts et il fournit quelques exemples de leur application.

L'Energie Atomique du Canada, Limitée
Etablissement de recherches nucléaires de Whiteshell
Pinawa, Manitoba, ROE 1LO

Juillet 1978

AECL-5991

ELASTIC PLASTIC FRACTURE MECHANICS

by

L.A. Simpson

ABSTRACT

The application of linear elastic fracture mechanics (LEFM) to crack stability in brittle structures is now well understood and widely applied. However, in many structural materials, crack propagation is accompanied by considerable crack-tip plasticity which invalidates the use of LEFM. Thus, present day research in fracture mechanics is aimed at developing parameters for predicting crack propagation under elastic-plastic conditions. These include critical crack-opening-displacement methods, the J integral and R-curve techniques. This report provides an introduction to these concepts and gives some examples of their applications.

Whiteshell Nuclear Research Establishment
Pinawa, Manitoba, ROE 1LO
July 1978

AECL-5991

CONTENTS

1. INTRODUCTION

Recent studies of the fracture behaviour of Zr-2.5% Nb pressure tube material have underlined a need to improve our understanding, within Atomic Energy of Canada Limited (AECL), of fracture mechanics in situations involving significant crack tip plasticity. To respond to this need and to an invitation from the Metallurgy Department at the University of British Columbia to lecture on the subject of elastic-plastic fracture, I have written this introductory appraisal of the field.

The fundamental purpose of fracture mechanics is to provide a framework by which a test result on a small specimen can be used to predict the loads under which a structure of the same material will fail by the propagation of an incipient flaw. Therefore, this framework must include a parameter which is a measure of the conditions of stress and strain at the crack tip, can be calculated from the applied forces on both the structure and test specimen, and signals the propagation of the crack at some identifiable critical condition. This parameter or fracture criterion must be geometry independent, that is, the failure conditions at the crack tip must be identical in both the laboratory specimen and in the structure itself.

Linear elastic fracture mechanics (LEFM) utilizes the critical stress intensity factor K_{Ic} as a fracture criterion for situations where crack propagation is accompanied by little or no plastic deformation. Quantitatively, this means that the extent of crack tip plasticity should be at least fifty times smaller than the dimensions of the structure, including crack length[1]. Because the extent of plasticity depends only on crack tip conditions and not significantly on specimen size, we find that larger structures may obey LEFM conditions while

small specimens of the same material may not. Thus a larger structure may exhibit brittle fracture behaviour while the small specimen fails in a ductile manner. Designating fracture amenable to LEFM as brittle, B, and elastic-plastic fracture as ductile, D, we can define four potential situations in fracture analysis involving a small specimen and a structure.

1. B-B - Both specimen and structure amenable to LEFM analysis, e.g. ceramics, brittle metals.
2. D-B - Specimen failure ductile, structure brittle, e.g. some high strength steels.
3. D-D - Neither specimen nor structure is amenable to LEFM analysis, e.g. CANDU* pressure tubes, pipeline steel.
4. B-D - Specimen brittle, structure ductile, a non-existent situation.

The principal applications for elastic-plastic fracture mechanics are in situations 2 and 3.

Although the bulk of this presentation is concerned with ductile crack propagation, it should be pointed out that failure in ductile materials can often be described more appropriately by theories of plastic collapse than by theories of crack propagation. Plastic collapse is failure by gross yielding of the specimen or structure and can be described by plastic limit analysis. Thus, failure is no longer localized to the crack tip region and may occur without any crack extension at all. In certain circumstances, plastic limit analysis will predict lower failure loads than some elastic-plastic crack propagation theories and must always be considered in ductile failure analysis.

---

* CANada Deuterium Uranium

2. SPECIMEN TYPES

While a fairly wide variety of fracture mechanics specimens has been developed with rigorous mathematical solutions for the elastic strain fields, the two most extensively used geometries in elastic-plastic fracture mechanics are the compact tension (CTS) specimen (including modifications such as the wedge opening load specimen) and the single edge-notched bend (SENB) specimen, Figure 1. For this discussion, these two will be used as the reference specimen geometries.

Figure 2 shows typical load-deflection curves for small specimens of various materials. Figure 2a depicts fully linear behaviour which is easily handled by LEFM and 2b shows "pop-in" behaviour characteristic of certain metals. Here LEFM can often be used to calculate K_{Ic} by the offset procedure as described by ASTM E399-72. Figures 2c and 2d illustrate the behaviour of concern in this presentation. Figure 2c shows considerable non-linear behaviour in the load deflection curve prior to sudden failure, while with the very ductile material in Figure 2d sudden failure never occurs. Obviously, this latter situation can occur only under displacement control. In fact, the shapes of curves 2c and d are as much a function of the testing arrangements (displacement control, load control, machine stiffness etc.) as of the material itself. The non-linearities can arise from two sources, plastic deformation at the crack tip and stable crack extension. The choice of approach in analyzing the fracture behaviour will depend on the amount of crack extension occurring prior to failure. It will also be necessary to define the point on the load-deflection curves at which failure is deemed to occur (measurement point). Some of the choices are (1) initiation of crack growth (stable or otherwise), (2) instability point under load control, (3) a critical amount of stable crack growth. This choice will depend on the degree of conservatism required and the geometry independence of the potential measurement points.

3. LIMITATIONS OF LEFM

To appreciate the need for an elastic-plastic fracture mechanics framework, the limitations of LEFM will first be reviewed. Figure 3 shows the crack tip region in a plane body where "a" is the crack length and "W-a" is the width of the uncracked ligament. We recall from LEFM that the stress intensity factor, K, is the coefficient of $(r/a)^{-1/2}$ in a power series in r/a which describes the stress field at a point a distance r from the crack tip. All other terms in the series are of order $(r/a)^{1/2}$ and higher; hence, when $r/a \ll 1$, the crack tip stress field can be described uniquely by K. Knott[1] shows quantitatively that, for $r/a < 0.02$, K describes the stress field with reasonable precision (region B in Figure 3). Because of the singular nature of the linear elastic stress field, a plastic zone forms at the crack tip where the yield condition for the specimen is exceeded (region A in Figure 3). Naturally K does not describe the stresses in the plastic zone because linear elasticity has been violated. Thus, if the plastic zone size is equal to or larger than region B, K loses its significance since it no longer uniquely describes the stress field anywhere in the body.

To summarize, for the stress intensity factor, K, to have significance, the in-plane dimensions a, W-a, must exceed the plastic zone size by a factor of 50.

Satisfaction of this criterion will ensure geometry independence for the in-plane stress components (equal stresses for equal K) but not for the stress component in the thickness direction. The latter is dependent on the degree of plane strain imposed near the crack tip by the effect of transverse constraint on thickness contraction of the plastic zone. If fully plane strain conditions apply to the structure under analysis, the test specimens, to be representative, must fail

under the same conditions. Hence we have the ASTM requirement for thickness, B, that

$$B > 2.5 \frac{K_{Ic}^2}{\sigma_y^2} \qquad (1)$$

where σ_y *is the yield stress.*

If the structure does not fail under fully plane strain conditions, K_c will be thickness dependent and an R-curve approach (to be described later) may be more suitable.

To summarize, to use plane strain fracture toughness, K_{Ic}, as a fracture criterion the ASTM thickness requirement must be met in specimen and structure in addition to the restrictions on in-plane dimensions.

4. PLASTIC ZONE CORRECTIONS

Historically, the first attempts at extending fracture mechanics beyond the LEFM limits described above involved making a correction to the crack length to allow for the effect of the plastic zone and continuing to use the LEFM approach. The early corrections proposed by Irwin[2] involved moving the crack tip to the center of the plastic zone, a distance r_y, i.e.

$$a \rightarrow a + r_y \qquad (2)$$

where $$r_y = \frac{1}{2\pi} \frac{K_c^2}{\sigma_y^2} \quad \text{(plane stress)}$$

$$= \frac{1}{6\pi} \frac{K_{Ic}^2}{\sigma_y^2} \quad \text{(plane strain)} \qquad (3)$$

The extra factor of 3 in the denominator for plane strain was somewhat arbitrarily chosen to allow for elevation of the yield stress at the crack tip by transverse constraint. The difficulty with this approach is that, while it often gives consistent results for small-scale yielding, the limits of its applicability are not clear. The very approximate nature of equation 3 is partially responsible for this.

More rigorous calculations of the plastic zone correction are available. The Dugdale[3] model is a useful example and will be discussed in some detail since the result provides the basis for much of the current work in the United Kingdom on elastic-plastic fracture mechanics. Dugdale assumed that yielding occurs in a strip-like zone at the crack tip which extends the crack by a distance c-a (Figure 4). The stresses in this yielded zone are considered to be a continuous distribution of point loads $\sigma_y.dt$ per unit thickness which act to restrain the crack from opening. By integrating the appropriate Westergaard stress function for point loads in cracks from a to c, an expression for the restraining stress intensity factor is obtained.

$$K = 2\sigma_y \left(\frac{c}{\pi}\right)^{1/2} \cos^{-1}\left(\frac{a}{c}\right) \qquad (4)$$

The size of the yielded zone is found by allowing equation 4 to oppose exactly the stress intensity factor for the opening of the crack under the applied stress σ and total crack length, c,

$$K = \sigma\sqrt{\pi c} \tag{5}$$

to give

$$\frac{a}{c} = \cos\frac{\pi\sigma}{2\sigma_y} \tag{6}$$

For $\sigma \to \sigma_y$, $a/c \to 0$ and general yielding spreads across the plate. For $\sigma/\sigma_y << 1$

$$a/c \to 1 - \frac{\pi^2\sigma^2}{8\sigma_y^2} \tag{7}$$

We can compare this with equation 3 as follows:

$$d_y = 2r_y = c-a \tag{8}$$

$$\therefore \quad \frac{a}{c} = \frac{a}{a+d_y} = (1 + \frac{d_y}{a})^{-1} \approx 1 - \frac{d_y}{a} + \ldots$$

for $d_y << a$.

Comparing this with equation 7,

$$r_y = \frac{d_y}{2} = \frac{\pi}{16}\frac{K^2}{\sigma_y^2} \tag{9}$$

This equation differs from the plane stress plastic zone size in equation 3 by about 20%.

An extension of the Dugdale analysis yields[4] an expression for the displacement normal to the crack plane at the crack tip, δ

$$\delta = \frac{8}{\pi} \frac{\sigma_y}{E} a \ln[\sec \frac{\pi\sigma}{2\sigma_y}] \quad (10)$$

which for $\sigma/\sigma_y << 1$ reduces to

$$\delta = K^2/\sigma_y E \quad (11)$$

The term δ is known as the crack opening displacement (COD) and is a useful measure of the crack tip strain.

The Dugdale analysis is one of plane stress. As before, plane strain situations can be handled by a modification to σ_y to account for yield stress elevation.

5. YIELD STRESS ELEVATION IN PLASTIC ZONES

The maximum shear stress in a body occurs on planes at 45° to the direction of the maximum and minimum principal stresses and is proportional to the difference between them. For instance, using the Tresca yield criterion

$$\sigma_{max} - \sigma_{min} = 2\tau_y = \sigma_y$$

where τ_y is the shear yield stress and σ_y is the uniaxial tensile yield stress. Referring to the stress components in Figure 5a, the thickness component in plane stress, σ_{33}, = 0 and

$\sigma_{22} = \sigma_y$ (Figure 5b).

However, in a triaxial stress system, $\sigma_{33} \neq 0$ and the stresses will be similar to those shown in Figure 5c. Because of the free surface at the crack tip, σ_{11} will rise from zero there and the yield condition will be

$$\sigma_{22} - \sigma_{11} = \sigma_y$$

$$\text{or} \quad \sigma_{22} = \sigma_y + \sigma_{11} \tag{12}$$

i.e. the stress component σ_{22} will exceed the uniaxial yield stress by an amount equal to σ_{11}. This elevation of stresses in the plastic zone can be as high as threefold in a perfectly plastic material and even higher for work-hardening materials[5].

Because higher stresses can be sustained, a crack may propagate by cleavage under plane strain but by a ductile process under plane stress where the cleavage stress is not attained. This underlines the importance of maintaining plane strain conditions in small specimens to predict plane strain failure in a structure. It will be seen in the following sections that certain approaches are capable of predicting plane strain behaviour using small specimens that violate the ASTM requirements (equation 1).

6. CRACK OPENING DISPLACEMENT

6.1 THE CONCEPT

Equation 10 gives an estimate of the crack-tip opening displacement under an applied stress. The concept that the crack will propagate upon attainment of some critical value of $\delta = \delta_i$ is a logical

one and we have seen in equation 11 that, for limited plasticity, δ_i is related to K_{Ic}. However, in many materials crack extension is stable under rising load to some much larger value of δ (= δ_{max}) before unstable failure occurs. It is in this latter circumstance that LEFM methods fail and a new approach is desirable.

An example of this stable crack extension is shown as the heat tinted surface in Figure 6. It initiates at the specimen mid-section where the level of transverse constraint is highest. Because the plastic zone size at the specimen surface is larger (Figure 7), the strain there for a given COD is more diffuse. Thus, ligaments remain, restraining further propagation of the stable crack unless the load is raised. As the load is raised, these plane stress ligaments penetrate more deeply, increasing the resistance to crack propagation, until fast fracture eventually occurs. Ultimate failure can occur at any stage or after a complete transition to slant fracture (full penetration of shear lips) depending on the material properties and specimen geometry.

The problem in using COD as a fracture criterion is in choosing the value at which "failure" occurs. The obvious choice for materials which do not show stable cracking behaviour is δ_i but materials which show it can often sustain much higher loads than that to reach δ_i and such an approach may be over conservative. However, the amount of stable crack growth a specimen will tolerate will depend on its thickness and δ_{max} will therefore be geometry dependent. Thus each case must be judged on an individual basis.

The geometry independence of δ_i was demonstrated by Knott[6] who tested SENB specimens of varying thickness. The δ_i values showed good agreement except for the 2 mm thickness which was less than two plastic zone diameters (3.4 mm). In this case, sufficient plane strain did not exist at the specimen mid-section to allow initiation at δ_i.

Knott[6] and others[7] have obtained good agreement between δ_i and K_{Ic} through equation 11, which is good evidence that initiation takes place under plane strain conditions. Thus, support is strong for the use of δ_i measurements (on small specimens) to predict plane strain failure (K_{Ic}) in structures where the ASTM requirements demand inconveniently large specimens.

In structures where full plane strain conditions are not maintained, the conservatism in using δ_i as a fracture criterion may be undesirable. If a higher value is used, a means of accommodating the geometry dependence must be found. Even maintaining constant thickness is not sufficient since δ_{max} appears to depend on crack length in otherwise identical specimens. The selection of the measurement point (critical value) of δ presents difficulties under these conditions since steel, at least, has been found to undergo slow crack extension at constant load where $\delta_i < \delta < \delta_{max}$[8].

It is not always a simple matter to relate COD in a structure to the applied loads and crack length, especially where the failure criterion is geometry dependent. Often direct calibrations will be necessary on the structure itself as was done in an early study on pressure tube fracture by the United Kingdom Atomic Energy Authority[9].

6.2 MEASUREMENT OF COD

While we have discussed at some length the applications of the COD approach, little has been said about how it is measured. The most common method employs a clip-on displacement gauge at the specimen crack mouth and a calibration between gauge reading and the actual crack tip displacement. It has been found for steels[10], using CT and SENB specimens, that after some initial loading, the crack faces separate as if there was a fixed center of rotation in the specimen ligament. This

center of rotation is determined experimentally by photographing pairs of microhardness indentations on the crack faces as the specimen is loaded. Sets of displacement readings, each corresponding to a given load level, are plotted against distance from the crack tip (Figure 8). Extrapolation of these plots to zero displacement yields the center of rotation. For steels, r, the center of rotation, was found to be 0.3† to 0.4 after some initial loading and was independent of crack length and specimen size. In such situations, δ can be calculated (Figure 8) from

$$\delta = \frac{Vg}{1 + (a+z)/r(W-a)} \qquad (13)$$

Before using this type of calibration, it should be confirmed for each material that r is geometry independent and independent of load level. This is not always the case; in fact zirconium alloys do not exhibit this behaviour[11].

Robinson and Tetelman[7] used a different technique for calibrating clip gauge readings. They infiltrated the crack mouths of SENB specimens at various load levels with catalytically hardening silicone rubber. When the rubber had set, they broke the specimens open and determined COD directly from the mould.

6.3 MEASUREMENT OF δ_i

Several methods are available for detecting the onset of stable crack growth so that δ_i can be determined from a test in which COD is monitored. Smith and Knott's technique[12], Figure (9), involves loading a series of specimens to various stages of the load-defection curve, unloading, marking the extent of stable crack growth by heat

---

† expressed as a fraction of the ligament size, W-a (see Figure 8).

tinting, and fracturing the specimen. The extent of stable crack growth is measured and plotted against crack opening displacement as in Figure (9). The zero intercept gives δ_i.

To be accurate, the above technique requires at least five specimens. In some materials, δ_i can be detected by measuring the electrical potential drop across a specimen in which a constant electric current is passed. The onset of stable crack growth gives rise to an abrupt change in the specimen resistance.

The term δ_i can also be measured directly from the fracture surface of a specimen[13]. Generally three regions are visible, the fatigue precrack and the stable crack surface are separated by a band of stretched material inclined about 45° to the crack plane. This is called a stretch zone and is a manifestation of the crack tip deformation during development of the crack opening displacement. The size of the stretch zone projected normal to the crack will be related to δ_i since the zone stops growing once stable crack extension begins. By averaging a number of measurements taken along the stretch zone, a good estimate of δ_i can be obtained. Again, the validity of this method must be confirmed for each material.

7. THE J INTEGRAL

7.1 DEFINITIONS

Consider a body containing a crack as in Figure 10. J.R. Rice[14] discovered in the 1960's that the following line integral has some very interesting properties when evaluated on a contour, Γ, enclosing the crack tip and running from the lower face to the upper face (Figure 10).

$$J = \int_{\Gamma} [W\, dy - Ti \frac{du_i}{dx} ds] \qquad (14)$$

where $W = \int_{o}^{\varepsilon} \sigma_{ij} d\varepsilon_{ij}$ (strain energy density for elastic materials),

T_i = tractions on the contour,

u_i = displacements on the contour.

Rice[14] demonstrated that for a body showing non-linear elastic behaviour, the value of J for a given set of loading conditions and crack geometry was independent of the path of integration. This implies that J is a crack tip parameter since a circuit taken just adjacent to the tip would give the same result as a circuit taken some distance out. Since it is a crack tip parameter, it can be evaluated at some distance from the crack tip where the deformation state is more accurately known. If we allow the crack to propagate a small increment, da, moving the contour with it, then $\int$ Wdy da is the change in strain energy moving to the new contour and $\int T_i\, du_i/dx\, ds\, da$ is the work done by the tractions in moving. Thus Jda is the total energy flow through the contour for an extension of the crack by da. Because of path independence, we can shrink the contour to one just surrounding the crack tip region and hence J is just the energy made available for crack extension, i.e., J = G, the strain energy release rate for linear or non-linear elasticity. Also for linear elasticity

$$J = G = \frac{K^2}{E} \quad . \qquad (15)$$

Another definition of J is derived below. Referring to Figure 11, the potential energy per unit thickness of a cracked body is given by

$$U = \int_A W \, dx \, dy - \int_{S_T} T.u \, ds \qquad (16)$$

where A is the in-plane area of the body and S_T is the surface over which tractions are prescribed. By comparing this with equation 14 and recalling that dx = -da

$$J = \frac{-dU}{da} \qquad (17)$$

i.e. J is equal to the change in potential energy with crack length. For non-linear elastic bodies, we can show that J is equal to the energy available for crack extension. Figure 11a shows a typical load, P, vs. defection, δ_p, curve for a specimen showing non-linear elastic behaviour. In the case of specified tractions (fixed load), equation 16 shows that the potential energy, U, is the shaded area in Figure 11a. When only displacements are specified (fixed grips), S_T becomes zero (i.e. it is non existent) and U is simply the strain energy or the area under the P-δ_p curve.

In Figure 11b, a specimen of crack length, a, is loaded to point A, and crack extension is allowed to proceed at fixed load to point B. The total work done on the specimen is area OABCO. Consider a hypothetical non-linear elastic specimen of initial crack length a+Δa loaded to point B. Its P-δ_p curve is obtained by unloading from B to C and is reversible. If we assume that the deformation states are the same in the two specimens at point B, the strain energy will be given by the area under the hypothetical curve. Then the energy available for crack extension in the actual specimen (work done-final strain energy) is the difference in the area under the two curves (shaded in Figure 11b). But this is the same as minus the difference in potential energies (areas above the curves as in Figure 11a). Thus, from equation 17, J is the energy available for unit crack extension.

For the fixed displacement case, Figure 11c, the strain energy is equal to the potential energy and the equality of ΔU to the energy available for crack extension (shaded area) is obvious. The small difference in shaded areas between Figures 11b and c is a second order infinitesmal and is negligible.

Using these results we have

$$J = -\frac{\Delta U}{\Delta a} = -\int_{\delta_p}^{\delta} \frac{dP}{da}\, d\delta_p = \int_{P}^{\partial \delta_p} \frac{}{\partial a}\, dP \qquad (18)$$

The derivations above apply to bodies showing non-linear elastic behaviour. Since our problem is to analyze elastic-plastic crack tip environments, we must justify such an extension. Rice proved the path independence of J for bodies obeying the laws of deformation plasticity. This theory relates <u>total</u> strain to the current state of stress and therefore lacks a history dependence. Thus loading in the body must increase monitonically everywhere and unloading, such as during stable crack extension, is prohibited. Since the load deflection curves of non-linear elastic bodies and those conforming to deformation plasticity theory are indistinguishable, equations 17 and 18 are exact for both cases. When plasticity is involved, J simply loses its significance as the energy available for crack extension because of the dissipative component of $\int W dy$. This is unfortunate but as we shall see in the next section J retains its significance as a crack tip parameter.

7.2 ELASTIC-PLASTIC CRACK TIP FIELDS

Figure 12 shows the crack tip region for a typical elastic-plastic body. In this view a large elastic-plastic field surrounds the crack tip which very near the crack tip will be an intensely non-linear zone associated with crack tip blunting. It is the well-behaved outer

elastic-plastic zone which we are concerned with. Just as K was found to describe the linear elastic near-tip stress field in LEFM, Hutchinson[15] and Rice[16] showed that the stress-strain field is described by,

$$\sigma_{ij} = \sigma_y \left(\frac{J}{r\sigma_y\varepsilon_y}\right)^{\frac{N}{N+1}} f_{ij}(r,\theta,N)$$
$$\varepsilon_{ij} = \varepsilon_y \left(\frac{J}{r\sigma_y\varepsilon_y}\right)^{\frac{1}{1+N}} g_{ij}(r,\theta,N) \qquad (19)$$

for material obeying a power law work-hardening relationship of the form (refer to stress-strain curve in Figure 12),

$$\sigma = \sigma_y \left(\frac{\varepsilon}{\varepsilon_y}\right)^N \qquad (20)$$

with σ_y, ε_y = yield stress and yield strain. Note that for the linear elastic case, N = 1, and equation 19 reduces to the familiar LEFM equations with $J = K^2/E$.

To summarize, J is the intensity of the elastic-plastic field surrounding the crack tip.

Just as the size of the plastic zone governs the validity of LEFM, so the size of the intensely non-linear zone restricts the applicability of J. Because of the intense deformations in this zone, accurate plasticity analysis is not possible. Rice and Johnson[5] have analyzed it using slip line theory. They show that it contains high hydrostatic stresses, at least three times the uniaxial yield stress. Paris[17] shows that if analysis using J is to be relevant, the size of this zone, $\bar{w}$, must satisfy

$$\bar{w} = 2\ J/\sigma_y \ll \text{planar dimensions.} \qquad (21)$$

Futhermore, if plane strain behaviour is to be maintained, the thickness B must satisfy

$$B \geq 25\ J/\sigma_y. \tag{22}$$

Note that this restriction is an order of magnitude less severe than the corresponding LEFM requirement in equation 1.

7.3 J AND COD

We have seen that J is fully consistent with the LEFM parameters G and K in elastic fracture conditions. We will now look at the interrelationship between J and δ.

We return to the Dugdale concept of a strip-like yielded zone at the crack tip. Barenblatt also considered this model but in a slightly different way (as described by Rice[18]) in that his restraining forces in the crack tip (cohesive) region were a function of δ, as in Figure 13. We calculate J by taking the integration contour just outside the cohesive zone, which is of negligible thickness, so that $dy \underset{\sim}{\sim} 0$. Then,

$$\begin{aligned} J &= -\int_{\Gamma} T_i \frac{\partial u_i}{\partial x}\, ds = -\int \sigma_{22} \frac{\partial}{\partial x} (U_2^{+} - U_2^{-})dx \\ &= -\int \sigma \frac{\partial \delta}{\partial x}\, dx = -\int \frac{\partial}{\partial x} \left[\int \sigma(\delta) d\delta\right] dx \\ &= \int_0^{\delta_t} \sigma(\delta)\, d\delta \end{aligned} \tag{23}$$

where δ_t is COD.

For the Dugdale model where $\sigma(\delta) = \sigma_y$,

$$J = \sigma_y \, \delta_t. \tag{24}$$

Again, in the limit of small scale yielding we have

$$J = G = \frac{K^2}{E} = \sigma_y \, \delta_t \tag{25}$$

which gives a consistent picture of the interrelationship of the various crack tip parameters.

The value of J is in its ability to serve as a geometry independent fracture criterion under much less stringent conditions of crack tip plasticity (equations 21 and 22) than LEFM methods. The most predominant application at present is in using small specimens, in which K_{Ic} cannot be determined, to determine a valid J. Equation 25 is then used to calculate K_{Ic} in thick structures where plane strain fracture occurs. Work in this area so far is very promising[19]. Its application to prediction of ductile fracture in structures, while not as well developed, seems attractive since J can be calculated for most structures as a function of crack size and loading by finite element analysis and equation 14. The suitability of this method, however, will depend on the demonstration of geometry independence for the critical J value and it may be more appropriate to use an R-curve technique as described in a later section.

7.4 APPLICATIONS OF J-INTEGRAL

We have seen that J is the change in potential energy in a specimen per unit increment of crack extension and can be calculated from the difference in areas under two load deflection curves for indentical specimens of slightly differing crack length. Begley and Landes[19]

used this definition to measure J_{Ic} on (sub ASTM size) compact tension specimens of low and medium strength steels. A series of specimens of differing crack lengths were loaded to failure and the load/load-point deflection curves were determined. At various stages of deflection the work expended (area under $P-\delta_p$ curve) was calculated and plotted against crack length as in Figure 14a. The slopes of these curves yielded $-dU/da = J$ and, using the set of curves, J was plotted as a function of δ_p in Figure 14b. It was fortuitous in this case that the critical deflection and hence the $J-\delta_p$ curve did not depend on crack length; however, this is not a restriction on the technique. The value of J at failure (crack initiation in this case) agreed very closely with K_{Ic} as determined on full thickness specimens (using equation 25).

The above method consumes a large number of specimens, which diminishes the advantage of using J to estimate K_{Ic} (small specimens). However, more recently, methods have been developed for determining J on certain single specimen geometries[20]. Consider a CT specimen of unit thickness deeply cracked so that deformation is primarily in bending. From equation 18,

$$J = \int_0^P \frac{\partial \delta_p}{\partial a} dP \tag{18}$$

For bending we substitute moment M for P and angular deflection θ for displacement.

$$J = \int_0^M \left(\frac{\partial \theta}{\partial a}\right)_M \partial M \tag{26}$$

where $\theta = \theta_{crack} + \theta_{no\ crack}$

θ_{crack} = deflection due to presence of crack

$\theta_{no\ crack}$ = deflection in absence of crack.

A dimensional argument shows that

$$\theta_{crack} = f\left(\frac{M}{(W-a)^2}\right) \tag{27}$$

where W-a is the uncracked ligament length. Then

$$-\frac{\partial\theta}{\partial(W-a)} = -\frac{\partial\theta_{crack}}{\partial(W-a)} = \frac{2M}{(W-a)^3} f'\left(\frac{M}{(W-a)^2}\right) \tag{28}$$

$$= \frac{2M}{W-a} \frac{\partial\theta_{crack}}{\partial M} \tag{29}$$

Substitution of 29 into 26 gives

$$J = \frac{2}{W-a} \int_0^{\theta_{crack}} M d\theta_{crack} \tag{30}$$

If the ligament forces are primarily bending (deep crack) but the moment is applied by a force P, we may substitute P, δ_p for M, θ,

$$J = \frac{2}{W-a} \int_0^{\delta_{crack}} P\, \delta_{crack} \tag{31}$$

Now for the deeply cracked CTS, $\delta_{crack} \approx \delta$ so that $\delta_{no\ crack}$ need not be determined and subtracted from the load displacement curve, thus,

$$J = \frac{2A}{W-a} \tag{32}$$

where A = area under the load displacement curve.

Generally, the requirement for deep cracks is satisfied if a/W > 0.6 although a more general expression of the requirement for deep cracks is that plasticity be confined to the ligament area.

Equation 32 is now widely used in determination of J values.

7.5 J AND STABLE CRACK EXTENSION

While the definition of J does not apply to situations where unloading occurs at the crack tip, there are at least two areas where it is desirable to extend J to this situation. One is cyclic fatigue at high load levels such that the LEFM description of cyclic load (ΔK) no longer is valid. Dowling and Begley[21] using A533B steel calculated ΔJ from the loading portion of the $P-\delta_p$ curve for each load cycle using equation 32. The crack growth correlated very well with valid LEFM data taken at lower load levels when both sets were plotted against ΔJ as in Figure 15. This is, therefore, strong evidence that the J integral may be adaptable to situations where unloading occurs.

Another area of interest is to calculate J in materials showing stable crack growth. When J at crack initiation provides an overly conservative failure criterion, it would be useful to be able to calculate it after a degree of crack extension. Garwood et al[22] suggested a method based on the assumption that J for a specimen in which the crack has extended from a to a + Δa (curve 1 in Figure 16) is the same as for a non-linear elastic specimen of initial crack length a + Δa and loaded to the same values of load and deflection. The actual and hypothetical load-deflection curves are shown in Figure 16. Initiation occurs at P and continues to point Q on curve 1. The energies U_1, U_2, U_3 and U_4 are represented by areas OPRS, ORQTS, OPQR, and PQTSR respectively.

$$\text{Now } U_1 + U_4 = U_2 + U_3 \tag{33}$$

From equation 32,

$$U_1 = \frac{J_o B}{2} (W-a_o) \tag{34}$$

$$U_2 = \frac{J_1 B}{2} (W-a_1) \tag{35}$$

The thickness B appears because equation 30 deals with unit thickness. J_o is the value of J at initiation and U_4 can be measured from the record so that J_1 can be calculated if U_3 is known. It is assumed that the U_3 energy is entirely consumed by crack growth, hence, for small Δa

$$U_3 = \frac{J_o+J_1}{2} B\Delta a \quad . \tag{36}$$

Substituting this back into equation 33 gives

$$J_1 = J_o \frac{W-a_1}{W-a_o} + \frac{2U_4}{B(W-a_o)} \tag{37}$$

Generalizing to successive increments of crack extension, we can calculate J_n, the value of J after the nth increment.

$$J_n = J_{n-1} \frac{W-a_n}{W-a_{n-1}} + \frac{2(U_n-U_{n-1})}{B(W-a_{n-1})} \tag{38}$$

This approach has yet to be proven theoretically sound but the success with the earlier fatigue correlations in unloading situations gives encouragement to this type of investigation.

We have seen that the J integral method is a very powerful technique for extending fracture mechanics beyond the LEFM boundaries. We have also seen that some of the theoretical limitations on its

validity may not be too severe. This is an active field of research at the moment with new developments appearing constantly. The reader should therefore be wary of applications applying some of the techniques to new or previously untested materials without very careful analysis including cross-checks of obtained J values against other fracture parameters for consistency, if possible.

8. R-CURVE TECHNIQUES

The J integral and COD methods discussed so far have shown their major successes in relating their values at the initiation of crack extension to K_{Ic} as measured in full-size structures which fail under plane strain conditions. We have seen much evidence that initiation occurs under plane strain conditions in small specimens which explains the success of COD and J in predicting K_{Ic}. However, many structures do not fail under fully plane strain conditions but will accomodate a significant amount of stable crack growth, usually under rising load. This is normally due to an increase in the proportion of plane stress fracture as the transverse stresses relax (described at the beginning of section 6). We have seen that δ_{max}, the COD at instability, can be much larger than that for initiation. Similarly, it appears from section 7.5, that J_n will continue to increase after crack initiation in some materials. Since these parameters will probably be geometry dependent after crack initiation, a new technique is required to normalize the results from various geometries. The R-curve has been proposed by many as a means of normalizing the failure behaviour of different geometries. The only restraint is that the specimen and the structure be of the same thickness.

Consider a CT specimen with in-plane dimensions sufficiently large that K describes the in-plane stresses but where the thickness is less than that required for plane strain fracture. Figure 17 shows a typical R curve for a specimen at initial crack length = a_o. As we load the specimen, K increases to point, P, at which stage crack initiation commences. As the crack extends further under rising load, K continues to rise until fast fracture occurs or it reaches a maximum. This plot of K vs crack extension is called the R-curve (for resistance curve) because it measures the resistance to further crack extension as a function of crack growth. K, so plotted, is often subscripted K_R and called crack growth resistance. There is a school of thought (and a considerable body of supporting evidence) which maintains that the R-curve is independent of specimen geometry for a given thickness of material. The fracture criterion used with R-curves states that when the strain energy release rate G (a,σ) is sufficient to cause instability, failure will occur. Thus, one plots a family of G-curves at various applied stresses σ_1, σ_2 etc. (converted to K_G, the crack driving force, via equation 25) as a function of crack length for the geometry in question. These are generally calculated from a stress analysis for the cracked structure. The stress σ_2 in Figure 17, just sufficient to give tangency between the G curve and the K_R curve, will be the critical failure stress for an initial crack length, a_o. Instability occurs because at tangency the energy release rate, K_G always exceeds K_R for futher crack extension. Because different geometries will have differently shaped K_G curves the point of tangency and hence the critical K_R value will be geometry dependent.

The need to express the R-curve in terms of K_R usually demands very large plate-like specimens to meet the in-plane dimensional requirements. Much of the current research on R-curves now is directed towards expressing crack growth resistance in terms of J or COD so that more

reasonable specimen sizes can be used. New ideas in this area are evolving almost daily so the reader is referred to the current literature for updating[11,21,22].

9. SUMMARY

The preceding has been an attempt to introduce to the reader, who is already familiar with basic LEFM concepts, some of the approaches for dealing with fracture of a more ductile nature. No claim for completeness is made, rather I have attempted to describe the more widely used approaches for dealing with elastic-plastic fracture. Some of the concepts are difficult to understand at first reading and the interested reader is advised to give careful study to the references cited in this work. I cannot hope to impart a full understanding of elastic-plastic fracture in these brief descriptions, but rather only hope to whet the reader's appetite for more knowledge.

REFERENCES

1. Knott, J.F., "Fundamentals of Fracture Mechanics", Wiley, New York, p. 134 (1973).

2. McClintock, F.A., Irwin, G.R., "Fracture Toughness Testing and its Applications", ASTM STP 381, American Society for Testing and Materials (1965).

3. Dugdale, D.S., J. Mech. Phys. Solids, 8, p. 100 (1960).

4. Bilby, B.A., Cottrell, A.H., Swinden, K.H., Proc. Roy. Soc. A272, p. 304 (1963).

5. Rice, J.R., Johnson, M.A., "Inelastic Behaviour of Solids", M.F. Kanninen, W.F. Adler, A.R. Rosenfield, R.I. Jaffee, eds., McGraw Hill, p. 641 (1970).

6. Knott, J.F., "Fundamentals of Fracture Mechanics", Wiley, New York, p. 162 (1973).

7. Robinson, J.N., Tetelman, A.S., "Fracture Toughness and Slow Stable Cracking", ASTM STP 559, Am. Soc. for Testing and Materials, p. 139 (1974).

8. Green, G., Knott, J.F., J. Mech. Phys. Solids, 23, p. 167 (1975).

9. Fearnehough, G.D., Watkins, B., Int. J. Fracture Mech., 4, p. 233 (1968).

10. Ingham, T., Egan, G.R., Elliot, D., Harrison, T.C., "Practical Applications of Fracture Mechanics to Pressure Vessel Technology", Inst. Mech. Eng., London, p. 200 (1971).

11. Simpson, L.A., Clarke, C.F., ASTM Symposium on Elastic-Plastic Fracture, Atlanta, Nov. 1977, to be published as an ASTM Special Technical Publication.

12. Smith, R.F., Knott, J.F., "Practical Applications of Fracture Mechanics to Pressure Vessel Technology", Inst. Mech. Eng., London, p. 65 (1971).

13. Simpson, L.A., Fracture 1977, 3, University of Waterloo Press, p. 705 (1977).

14. Rice, J.R., J. Appl. Mech. (Trans. ASME), p. 379 (June 1968).

15. Hutchinson, J.W., J. Mech. Phys. Solids 16, p. 13 (1968).

16. Rice, J.R., Rosengren, G.F., ibid., p. 1.

17. Paris, P.C., "Flaw Growth and Facture", ASTM-STP 631, p. 3, 1976.

18. Rice, J.R., "Fracture", H. Liebowitz ed., Academic Press, 2, p. 234 (1968).

19. Begley, J.A., Landes, J.D., "Fracture Toughness", ASTM STP 514, Am. Soc. for Testing and Materials, p. 1 (1972).

20. Rice, J.R., Paris, P.C., Merkle, J.G., "Progress in Flaw Growth and Fracture Toughness Testing", ASTM STP 536, Am. Soc. for Testing and Materials, p. 231 (1973).

21. Dowling, N.E., Begley, J.A., "Mechanisms of Crack Growth", ASTM STP 590, Am. Soc. for Testing and Materials, p. 82 (1976).

22. Garwood, S.J., Robinson, J.N., Turner, C.E., Int. J. of Fracture, 2, p. 528 (1975).

23. McCabe, D.E., 10th National Symposium on Fracture Mechanics, Philadelphia, Pa., 1976, to be published as an ASTM STP.

24. Garwood, S.J., Turner, C.E., "Use of the J-integral to Measure the Resistance of Mild Steel to Slow Stable Crack Growth", in Fracture 1977, Vol. 3, D.M.R. Taplin ed., U. of Waterloo Press, Waterloo, Canada.

T-7-19

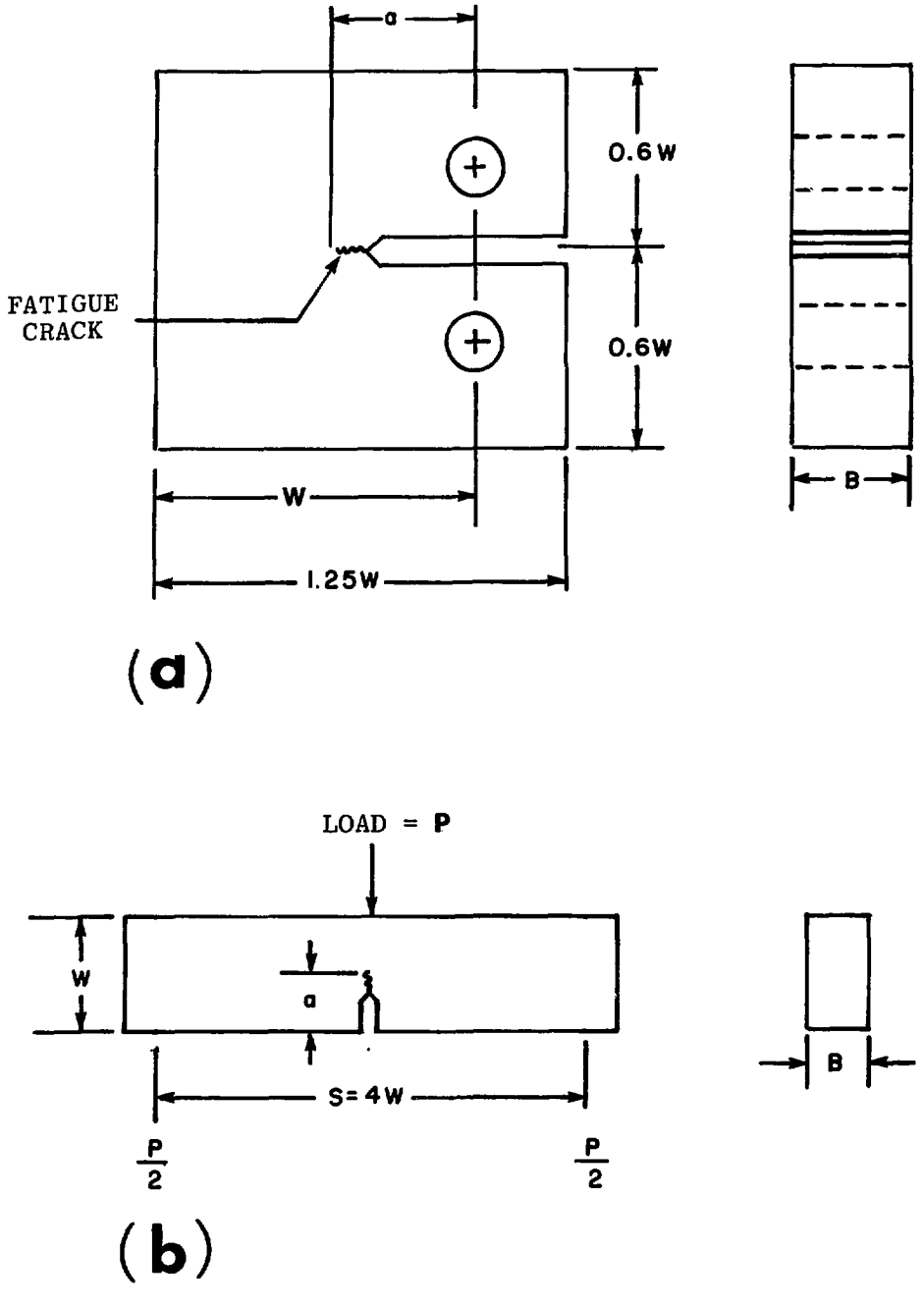

FIGURE 1: Compact Tension Specimen (a) and Single-Edge Notched Bend specimen (b) showing dimensions in standard (ASTM) nomenclature.

T-7-18

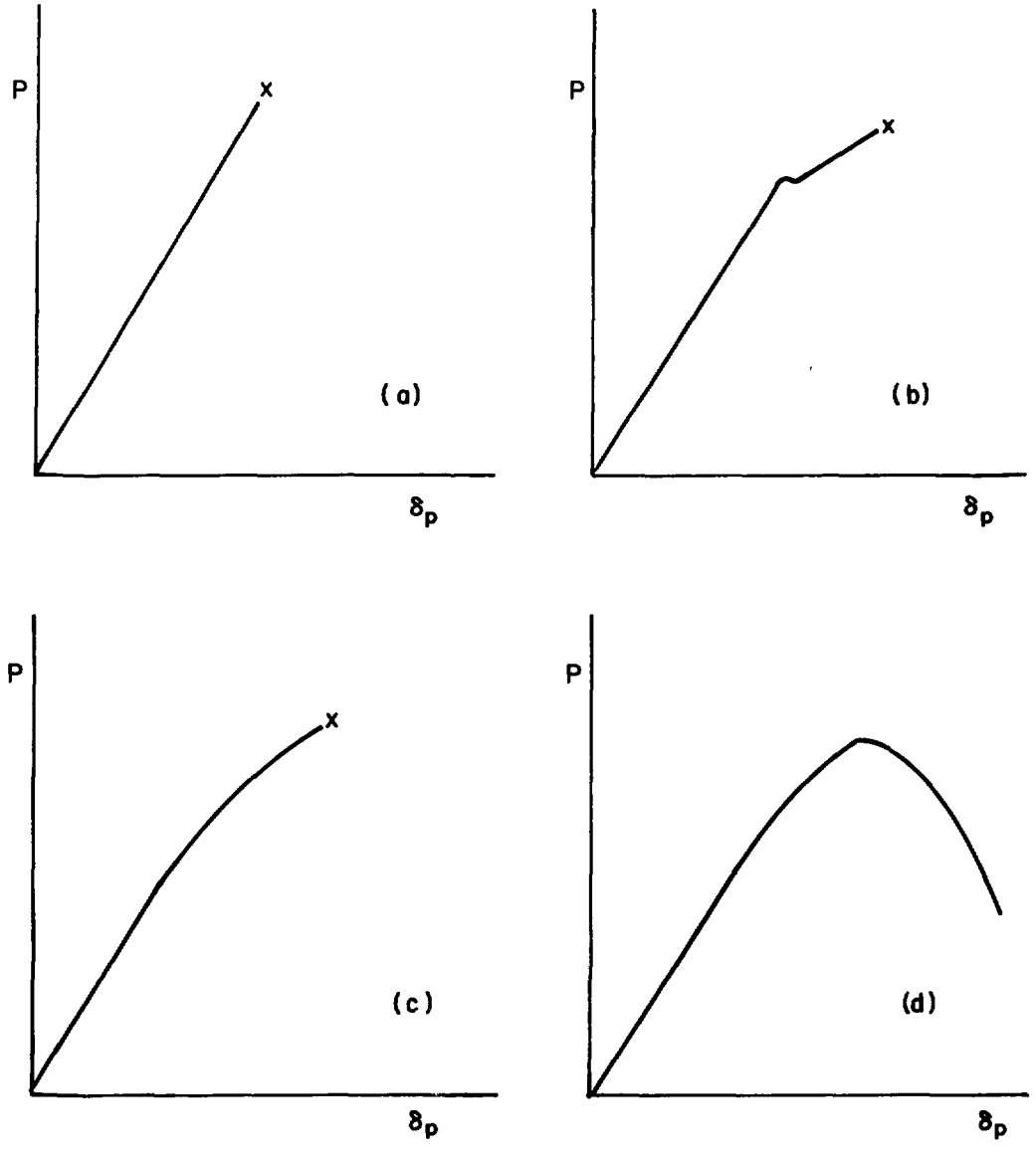

FIGURE 2: Schematic load (P)-load point deflection (δ_p) curves for fracture mechanics specimen with increasing amounts of ductility.

$$\sigma_{yy} = \frac{K}{\sqrt{2\pi r}} f(\theta) + \text{higher order terms in } r/a$$

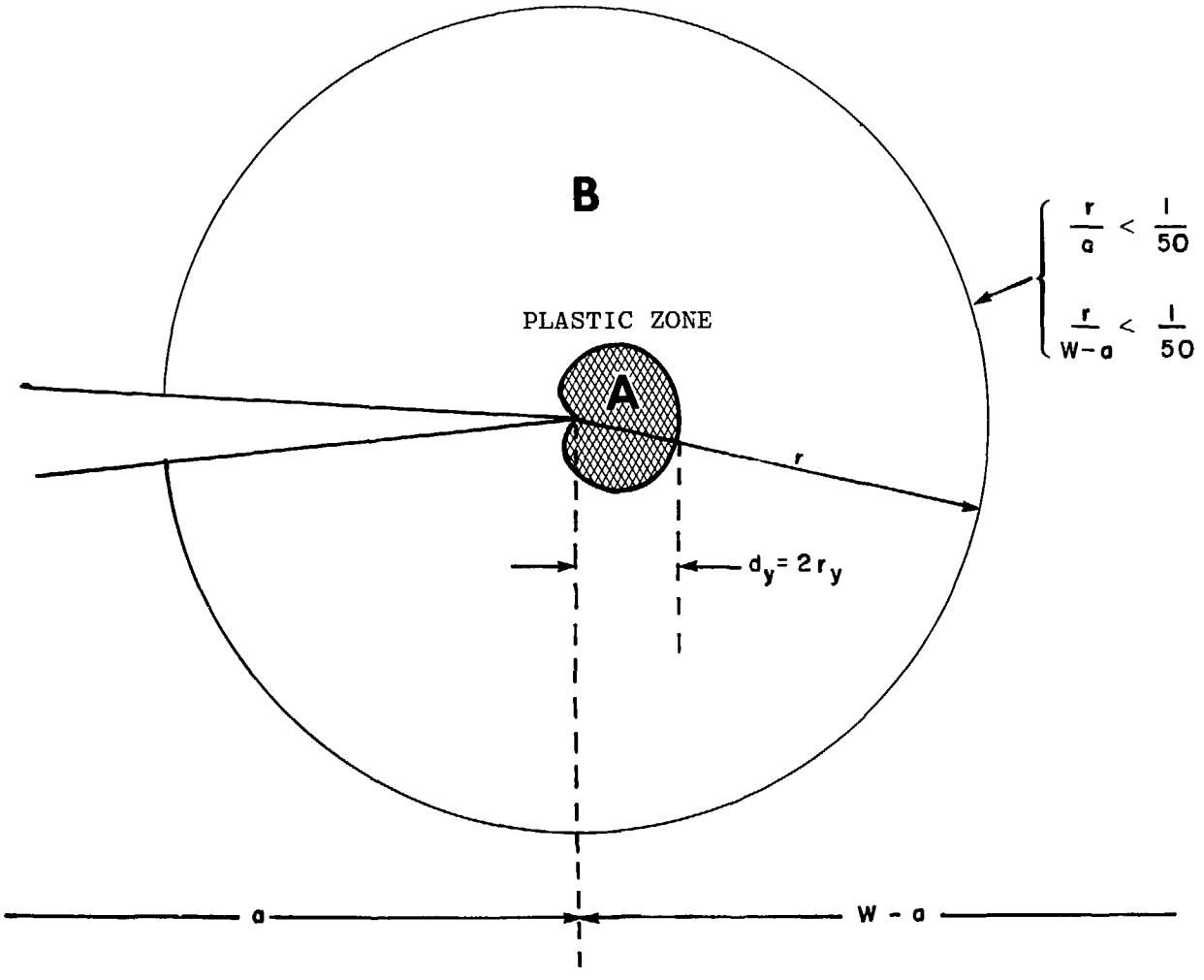

FIGURE 3: Crack tip region where K provides a one-parameter description of the stress field. a, W as in Figure 1.

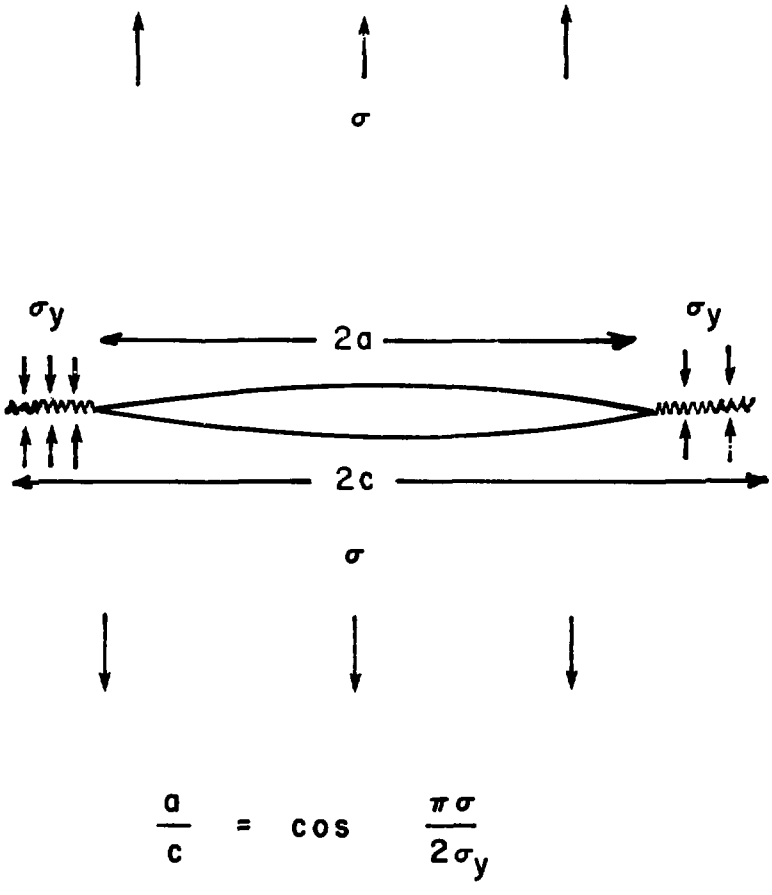

$$\frac{a}{c} = \cos\frac{\pi\sigma}{2\sigma_y}$$

FIGURE 4: Dugdale model of "strip-yield" plastic zones under applied stress σ. Plastic zone size is c-a.

T-7-15

a

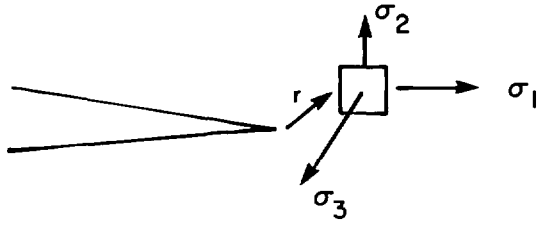

b PLANE STRESS

$\sigma_3 = 0$

$\sigma_2 - \sigma_3 = \sigma_2 \equiv \sigma_y$

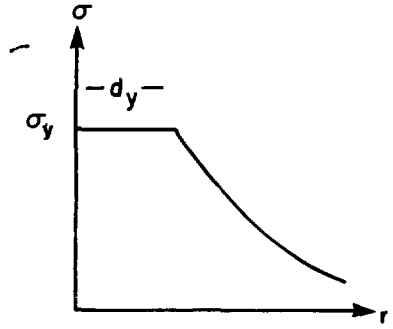

PLASTIC ZONE RADIUS $r_y = \frac{d_y}{2} = \frac{1}{2\pi} \frac{K^2}{\sigma_y^2}$

c PLANE STRAIN

$\sigma_3 \neq 0$

$\sigma_2 - \sigma_1 = \sigma_y$

$\sigma_2 = \sigma_y + \sigma_1$

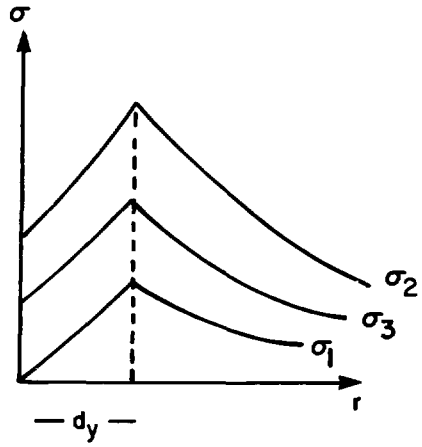

P.Z.R. = $r_y = \frac{1}{6\pi} \frac{K^2}{\sigma_y^2}$

FIGURE 5: Crack tip stress fields in plastic zone region as a function of distance, r, from the tip.
(a) Coordinates
(b) Plane stress
(c) Plane strain

FIGURE 6: Fracture surface of Zr 2.5% Nb CTS which has undergone stable crack extension (region S).

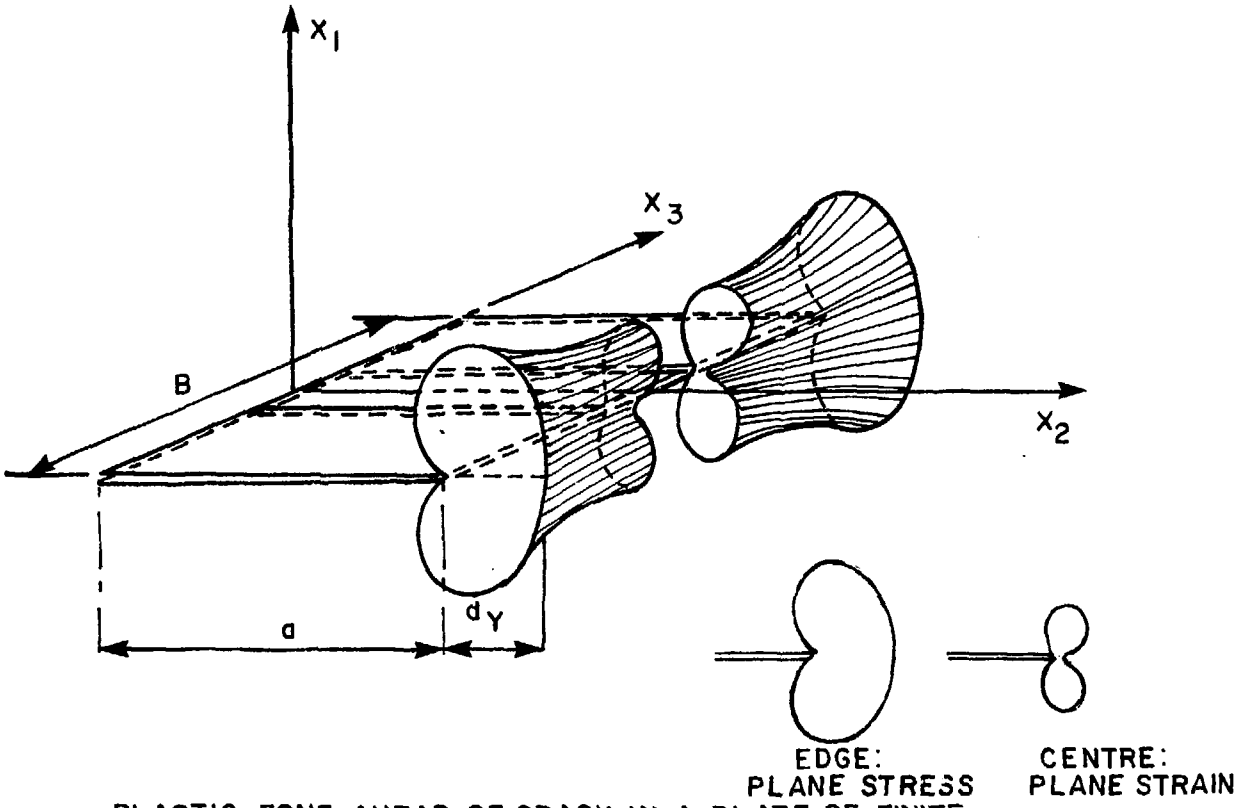

FIGURE 7 Shape of the plastic zone through the test specimen thickness Reproduced with permission, from Fundamentals of Fracture Mechanics, p. 120, John Wiley and Sons, Inc. (reference 1).

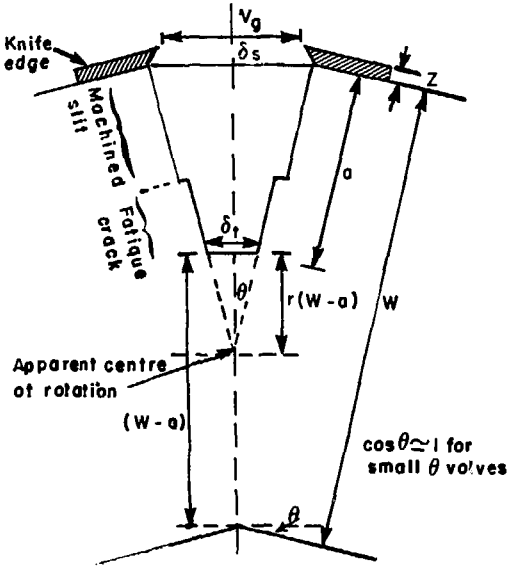

REPRESENTATION OF NOTCH PROFILE DURING BENDING

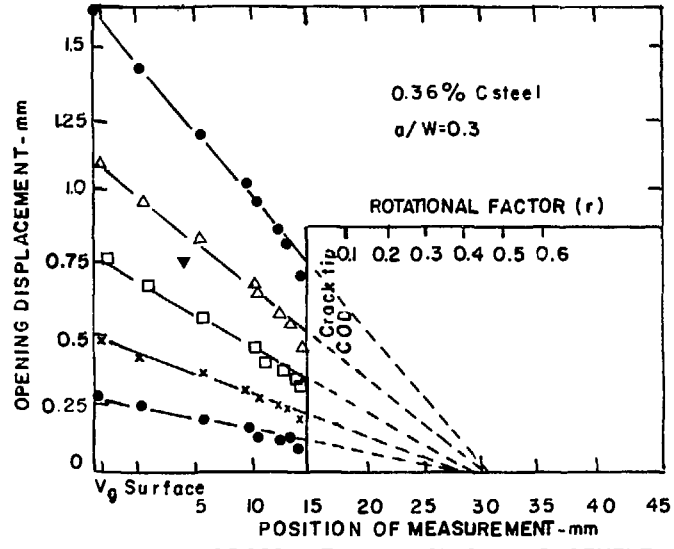

VARIATION OF COD WITH POSITION OF MEASUREMENT FOR A 25mm x 51mm BEND TEST, 0.36% C STEEL

FIGURE 8: Method of calibrating clip gauge reading to give COD based on a fixed center of rotation
Reprinted by permission of the Council of the Institution of Mechanical Engineers from Practical Applications of Fracture Mechanics to Pressure Vessel Technology (reference 10).

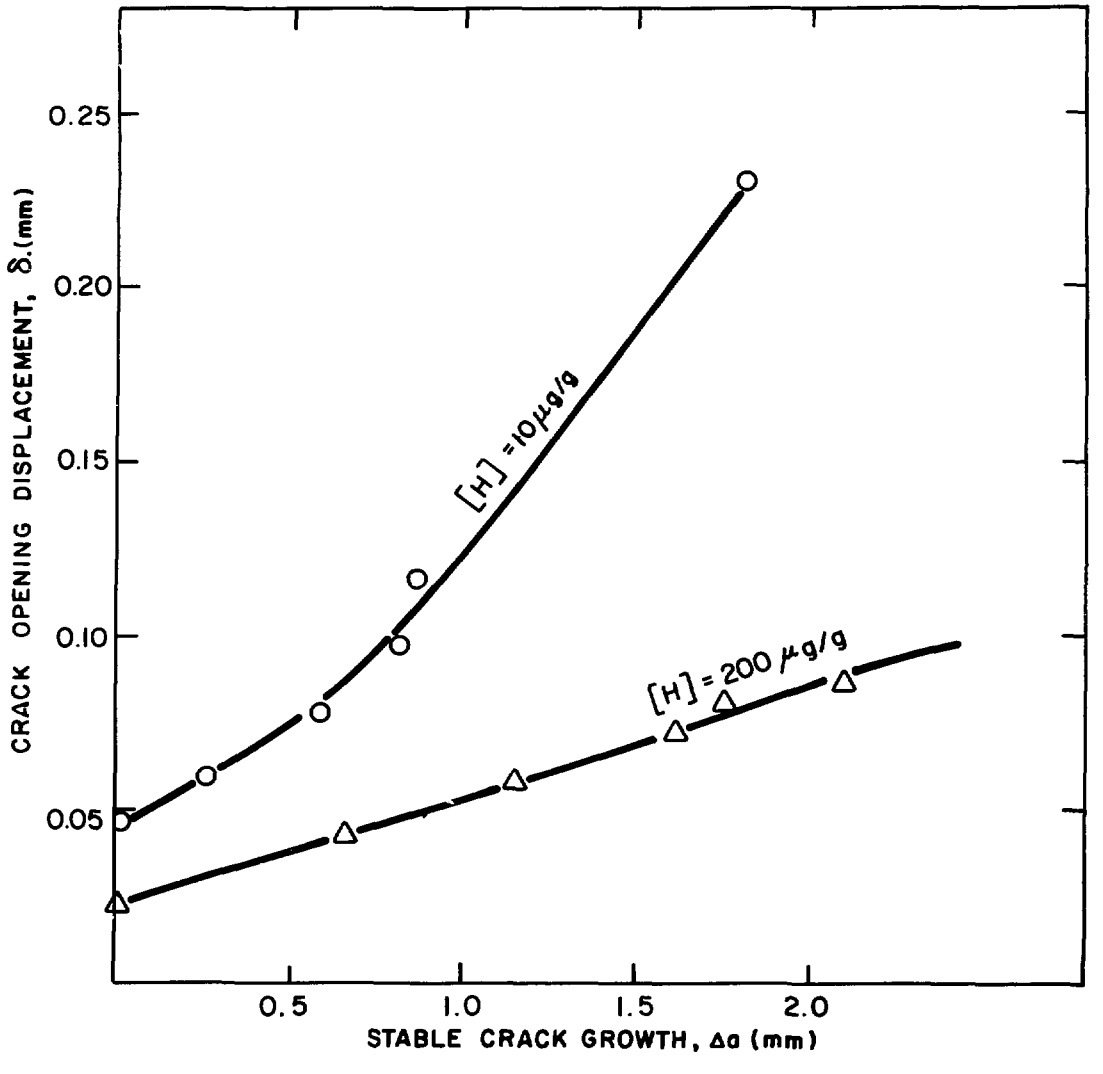

FIGURE 9: Application of the Smith and Knott method of determining δi to Zr 2.5% Nb pressure tube material[13] (CT specimens).

T-7-14

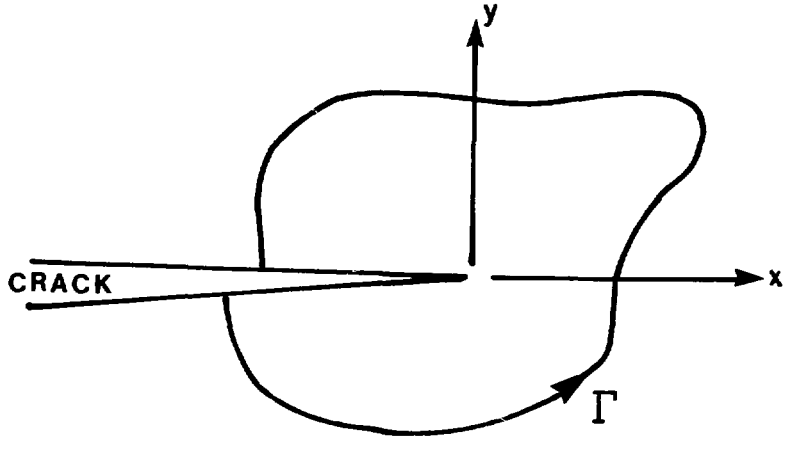

FIGURE 10: Typical path of integration, Γ, used in calculating the J-integral.

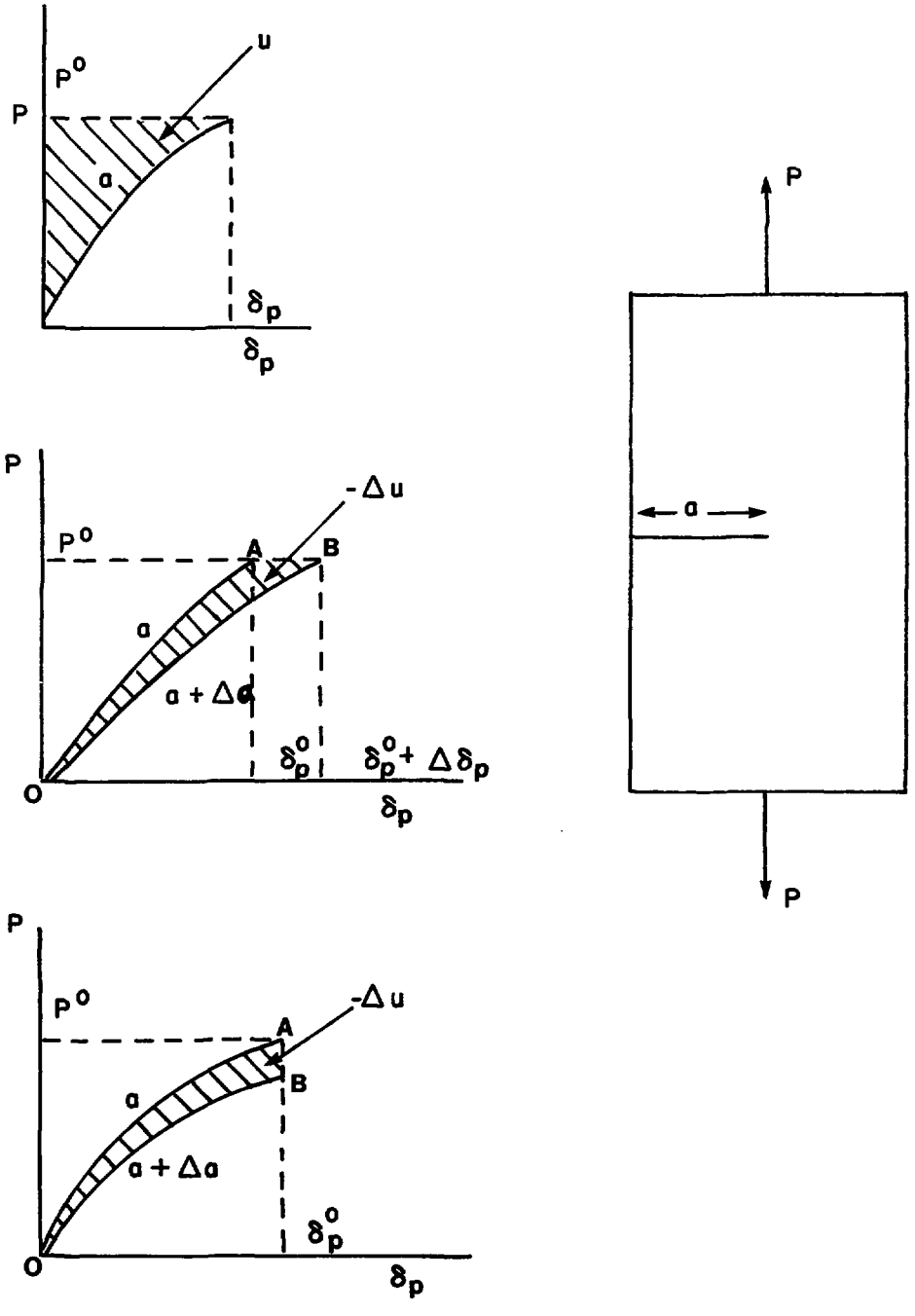

FIGURE 11: Load (P) point deflection (δ_p) curves showing potential energy changes with crack extension (Reference 17)

(a) U for situation where tractions are prescribed (fixed load)
(b) ΔU for fixed load case
(c) ΔU for fixed displacement case.

$$\sigma_{ij} = \sigma_y \left(\frac{J}{r \sigma_y \epsilon_y} \right)^{\frac{N}{N+1}} f_{ij}(r\ \theta\ N)$$

PLASTIC FIELD

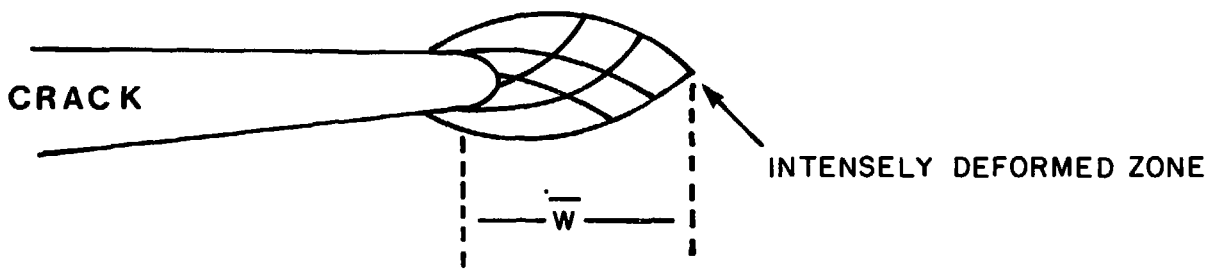

$$\overline{W} \approx 2\ \frac{J}{\sigma_y} << a,\ W - a$$

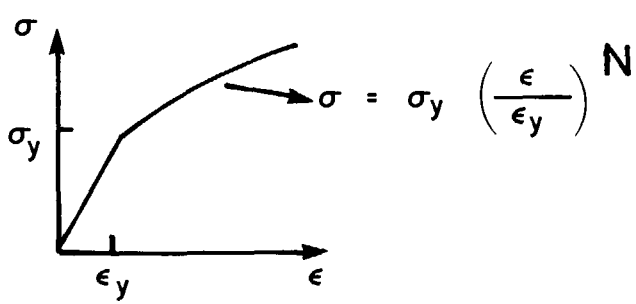

FIGURE 12: Elastic plastic crack tip deformation fields.

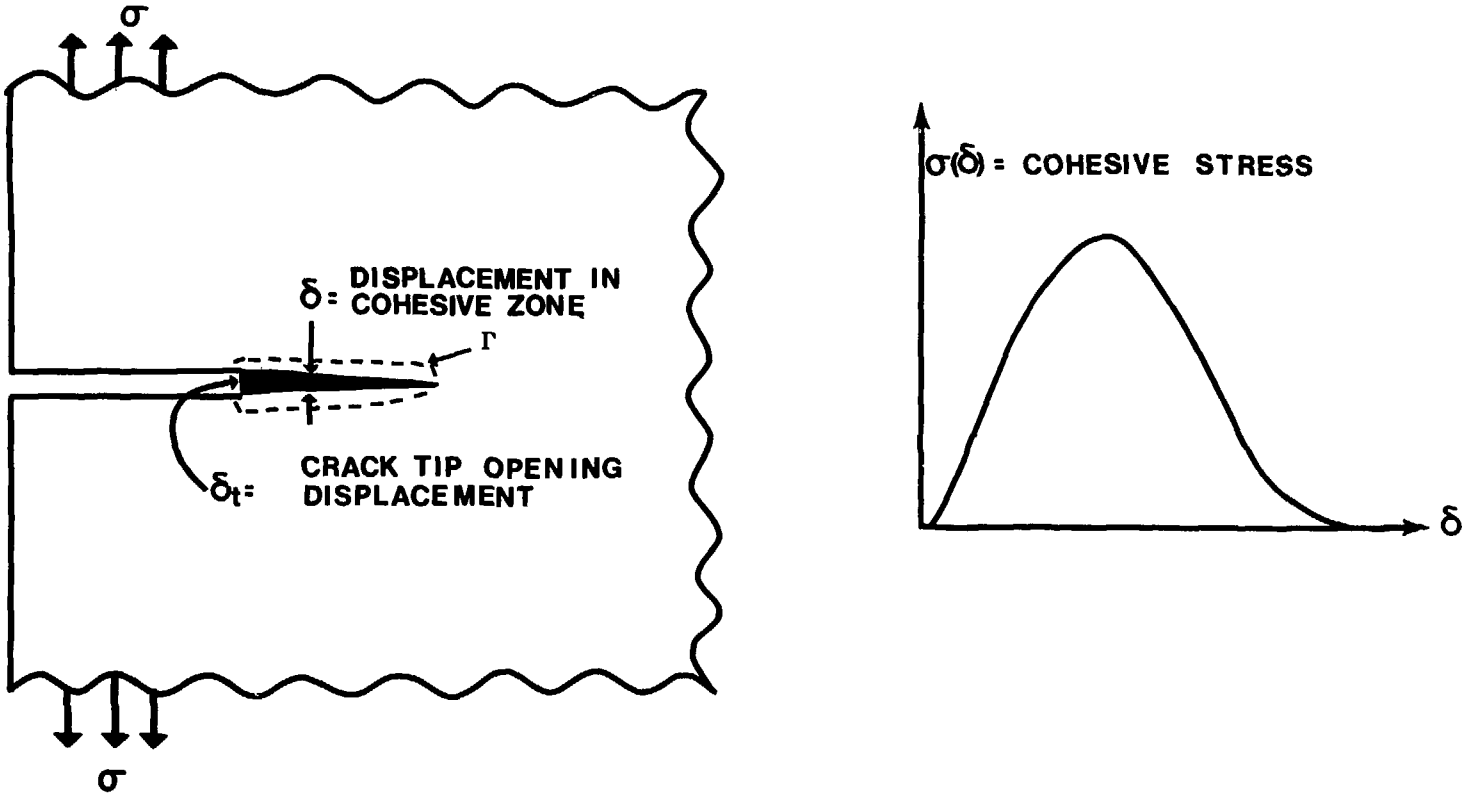

FIGURE 13: Barenblatt cohesive force model of a crack tip showing circuit for J calculation

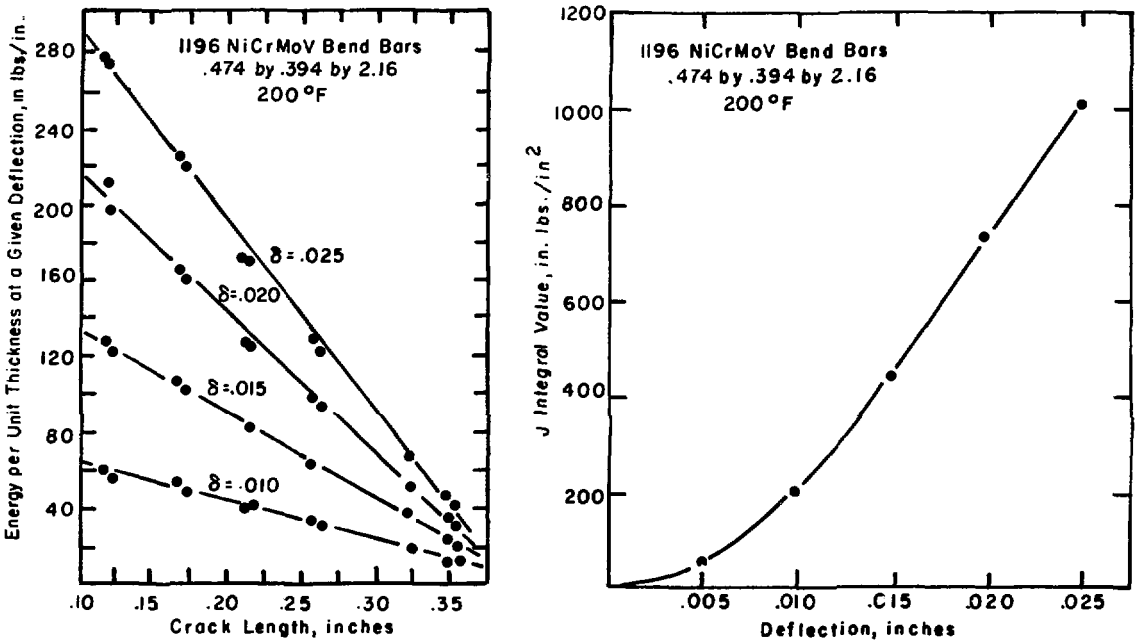

FIGURE 14: J-integral determination on steel by Begley and Landes[19]
(a) Energy adsorbed at a given deflection versus crack length
(b) J volume as a function of deflection
Reprinted by permission of the American Society for Testing and Materials, copyright.

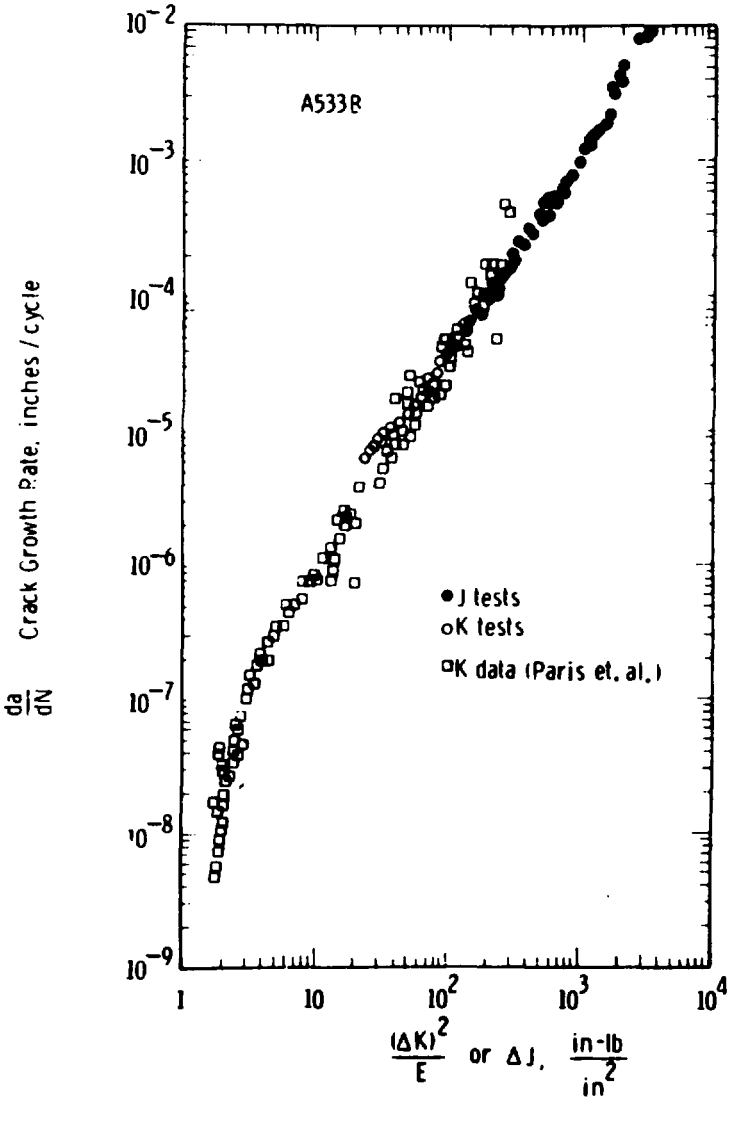

FIGURE 15: Comparison of fatigue crack growth rates during gross plasticity with linear elastic data[21].
Reprinted by permission of the American Society for Testing and Materials, copyright.

T-7-12

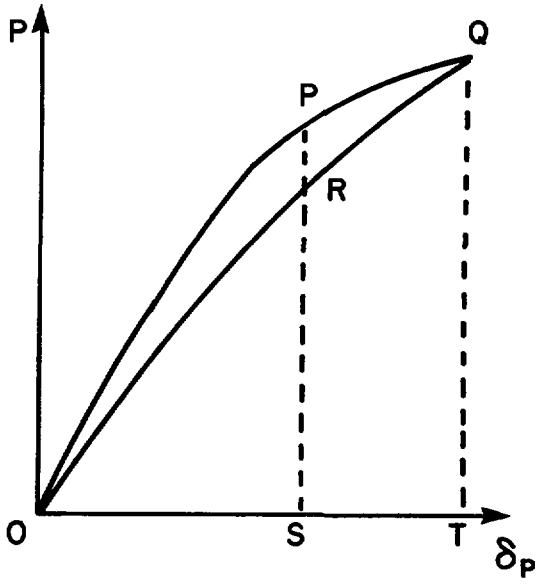

FIGURE 16: Actual (OPQ) and hypothetical (ORQ) load-deflection curves for determination of J subsequent to stable crack growth.

-7-11

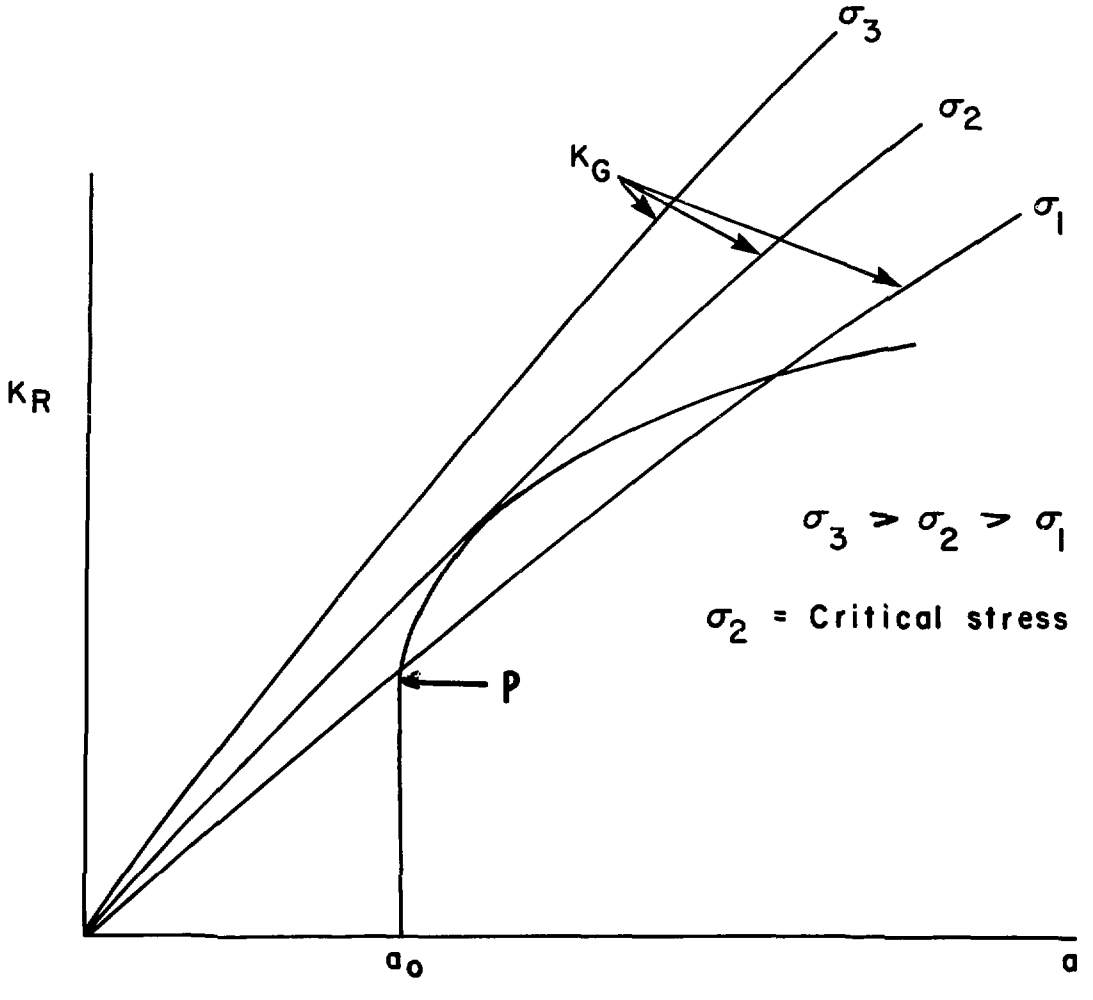

FIGURE 17: Matching of an R curve to crack driving force curves to determine the critical stress.

The International Standard Serial Number

ISSN 0067–0367

has been assigned to this series of reports.

To identify individual documents in the series
we have assigned an AECL–number.

Please refer to the AECL–number when
requesting additional copies of this document
from

Scientific Document Distribution Office
Atomic Energy of Canada Limited
Chalk River, Ontario, Canada
K0J 1J0

Price - $4.00 per copy

1534-78